Zeitschrift: Schweizerische mineralogische und petrographische Mitteilungen = Bulletin suisse de minéralogie et pétrographie

Band: 84 (2004)

Heft: 1-2: Geodynamics and Ore Deposit Evolution of the Alpine-Carpathian-Balkan-Dinaride Orogenic System

Artikel: LA ICP-MS study of fluid inclusions in quartz from the Yuzhna Petrovitsa deposit, Madan ore field, Bulgaria

Autor: Kostova, Bilyana / Pettke, Thomas / Driesner, Thomas

DOI: https://doi.org/10.5169/seals-63737

Schweizerische Mineralogische und Petrographische Mitteilungen 84, 25–36, 2004

LA ICP-MS study of fluid inclusions in quartz from the Yuzhna Petrovitsa deposit, Madan ore field, Bulgaria

Bilyana Kostova[1,*], *Thomas Pettke*[2], *Thomas Driesner*[2], *Paraskev Petrov*[1] and *Christoph A. Heinrich*[2]

Abstract

Major and trace elements contents of individual fluid inclusions in quartz from the Yuzhna Petrovitsa hydrothermal Pb–Zn deposit were analyzed microthermometrically and by LA ICP-MS in order to better characterize the ore-forming fluids and their evolution. We found different trends in T_h vs. depth for fluid inclusions associated with various stages of mineralization, which quantitatively match predictions from published hydrothermal fluid flow simulations. The data indicate that the early quartz–pyrite association formed when the hydrothermal system was still heating up. The somewhat later quartz–galena–sphalerite main ore stage was deposited during the thermal peak under hot hydrostatic head conditions with a temperature-depth distribution representing the fluid's boiling curve, and post-sulphide quartz formed after the thermal peak. Galena and sphalerite precipitated from a slightly acid fluid with a Pb content of about 7–8 ppm and a Zn content of about 33 ppm at the present-day +668 m level, which represents a paleodepth of about –1200 m. Precipitation within the vein structure was mainly the result of cooling from about 310 °C to 285 °C over the investigated 400 m vertical interval. Ore fluid concentrations of lead and zinc can be used to estimate a minimum time-integrated amount of fluid in the order of 10^2 km^3 that was necessary to form the Madan ore field, which agrees well with typical values for present day hydrothermal systems.

Keywords: Hydrothermal, fluid inclusions, LA ICP-MS analysis, Madan, Bulgaria.

Introduction

Major Oligocene lead-zinc mineralization in the Central Rhodopes occurs in four ore fields: Madan, Laki, Davidkovo (South Bulgaria) and Thermes (Greece). The host rocks of the ore fields are migmatized orthogneisses, schists, amphibolites and marbles of the Arda tectonic unit and Madan and Startsevo Allochthone (Fig. 1). The Arda unit represents the lower plate, and the Madan and Startsevo Allochthone the upper plate of an extensional structure, the Central Rhodope or Madan dome. The Madan ore field is located in the southwestern part of the dome. Paleogene sediments are situated in the NW part of the ore field (Ivanov, Dimov and Sarov, 2000). Rhyolites form several dikes in the northern part. U–Pb dating on zircons of the dikes defined their emplacement at 32–30 Ma ago (Ovtcharova et al., 2002). The dikes crosscut the extensional faults indicating that magmatism took place after the main extensional event.

Thirty-nine lead–zinc deposits were mined within the Madan field (Kolkovski and Dobrev, 2000). The larger deposits are related to six fault zones with lengths up to 15 km and more. The ore bodies are of three types – veins, carbonate replacement bodies and stockworks. Veins are the most widespread with typical lengths between 500 m and to 2 to 2.5 km and vein widths up to 10 m (more commonly 1–2 m). Ar–Ar measurements of sericite associated with the main Pb–Zn mineralization reveal mica crystallization ages of 30.5–29 Ma (Rohrmeier et al., 2002) in agreement with the observation that the ore veins crosscut the rhyolitic dikes in some areas. Fault zone-bound stockworks are not abundant and mainly occur in the deposits in the southern part of the ore field. Carbonate replacement ore bodies were formed where the ore-bearing faults cut the marbles. The thickness of metasomatic ore bodies is controlled by the thickness of marble layers and usually is 4–5 m. The main minerals of all deposits are quartz, galena and sphalerite with additional johannsenite becoming important in the peripheral parts of the replacement ore bodies. In decreasing order of abundance, additional ore minerals are pyrite, chalcopyrite and arsenopyrite, and as gangue

[1] Department of Mineralogy, Petrology and Economic Geology, Sofia University, "St. Kliment Ohridsky", 15 Tsar Osvoboditel Bd., BG-1504 Sofia, Bulgaria.
[*] Present address: CLMC "Acad. I. Kostov", Bulgarian Academy of Science, Acad. G. Bonchev str., bl. 107, BG-1113 Sofia, Bulgaria. <bilyana@clmc.bas.bg>
[2] Institute of Isotope Geochemistry and Mineral Resources, ETH-Zentrum, CH-8092 Zürich, Switzerland.

0036-7699/04/0084/25

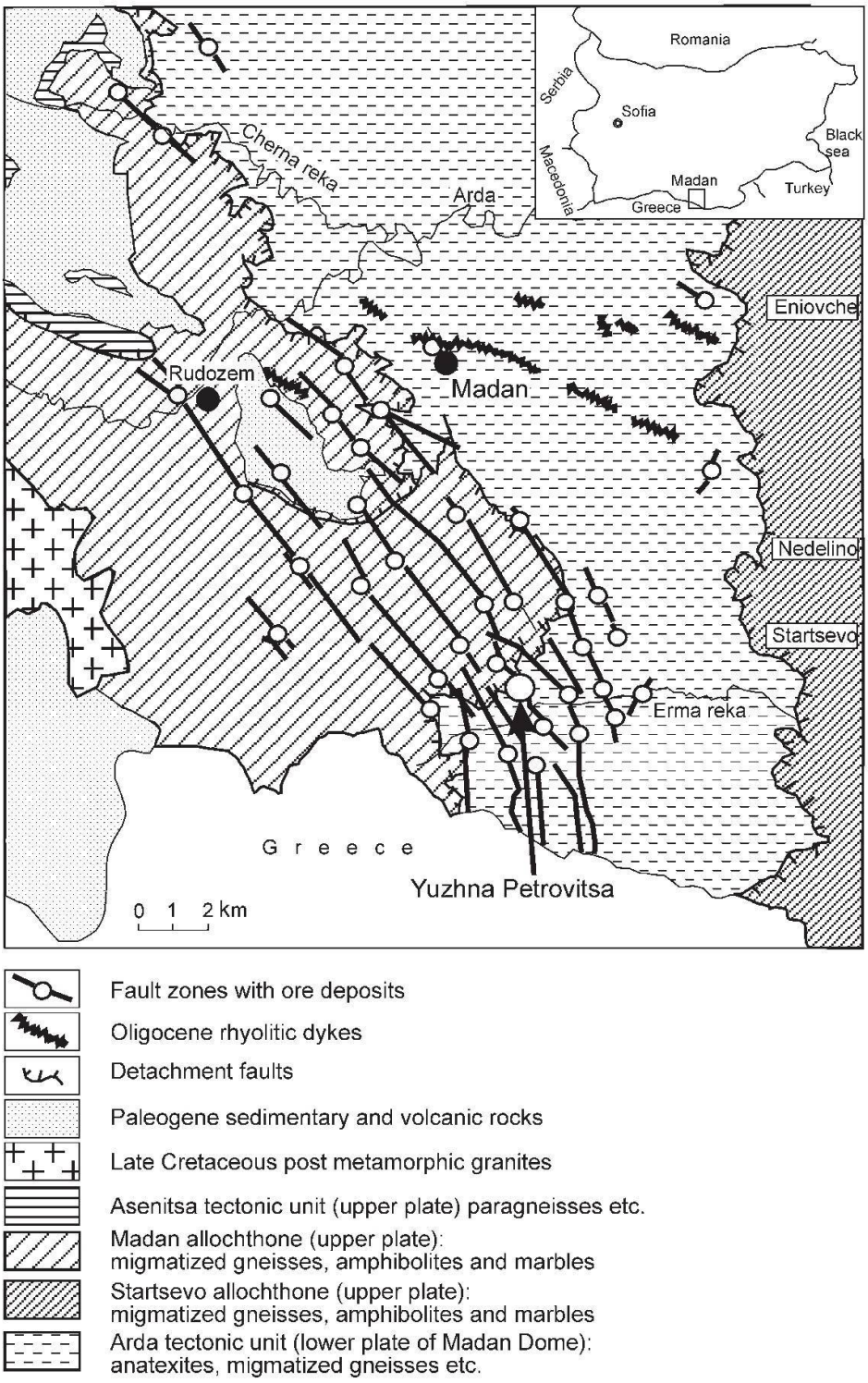

Fig. 1 Simplified geological map of the Madan ore field (after Ivanov et al., 2000).

minerals calcite, manganocalcite, rhodochrosite, dolomite and rhodonite, the last occurring in the metasomatic ore bodies only. One of the most important faults for ore-localization is the Karaaliev dol-Petrovitsa fault on which the Yuzhna Petrovitsa deposit of this study is located (Fig. 1). We chose this specific mine for a case study because well-documented samples of the major mineralization stages were available over a >400 m vertical interval.

The Madan ore field is of particular interest for the study of hydrothermal ore formation because large primary fluid inclusions are abundant in the sulphide ore minerals (Bonev, 1977; Bonev and Kouzmanov, 2002). These inclusions frequently reach a size that allows sampling for classical wet-chemical analysis. The pioneering work of Bonev (1977), Piperov et al. (1977), and Piperov and Penchev (1982) showed dominantly meteoric water with generally low salinities and NaCl

as the main solute. The inclusions contain CO_2-bearing vapour bubbles of variable volume fraction, indicating that the ore-forming fluid was boiling. Quantitative data on Na, K, Ca, Fe, Mn, Cl^- and δD, as well as upper limits for Mg, Pb, Cu, Zn, Al, F^-, HCO_3^-, SO_4^{2-}, HS^-, and S^{2-} were obtained in these studies.

While this was a major achievement in characterizing the general nature of the ore-forming fluids, it was not possible to analytically determine the original ore metal content of the fluids because of post-entrapment deposition on the sulphide inclusion walls. This original ore metal content, however, should be preserved in fluid inclusions in cogenetic or previously deposited quartz. It is now possible to quantitatively analyze these with the LA-ICPMS method (Günther et al, 1998; Heinrich et al., 2003). In addition, quartz also contains fluid inclusions from pre- and post-ore stages, thus allowing the study of thermal and chemical fluid evolution in detail. The study of Kolkovski and Petrov (1972) showed that systematic trends in the thermal evolution of the system are recorded in quartz-hosted inclusions from several deposits in the Madan area.

The primary goals of this study were to determine the salinity and temperature distribution as well as possible variations of major, ore and other trace elements in single fluid inclusions from quartz crystals associated with the various stages of ore deposition over the vertical extent of the Yuzhna Petrovitsa mine.

Sample material and methods

Fluid inclusions in vein quartz as well as in quartz from metasomatic replacement bodies from the Yuzhna Petrovitsa deposit were studied. The fluid inclusion measurements reported here are based on 11 carefully selected samples that represent a 460 m vertical interval of the deposit (Fig. 2).

The investigated quartz belongs to different mineralization stages. According to Kolkovski and Dobrev (2000), 6 paragenetic stages can be distinguished: (1) quartz–pyrite, (2) quartz–galena, (3) quartz–galena–sphalerite, (4) rhodochrosite–dolomite–manganocalcite, (5) quartz–arsenopyrite+/–sulphosalts, and (6) manganocalcite–calcite, not all of which are present in all parts of all mines.

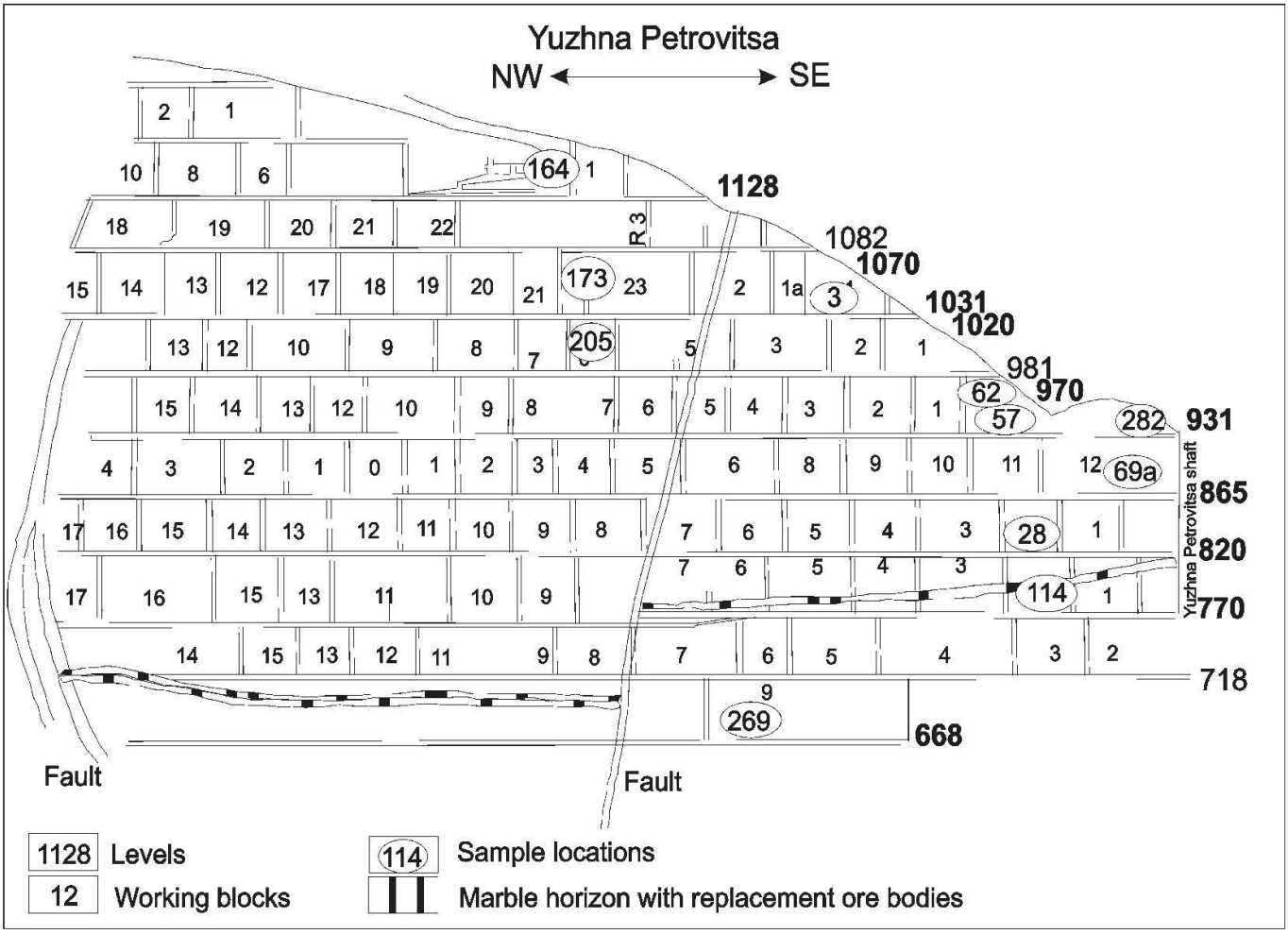

Fig. 2 Sample location within the Yuzhna Petrovitsa Pb–Zn mine.

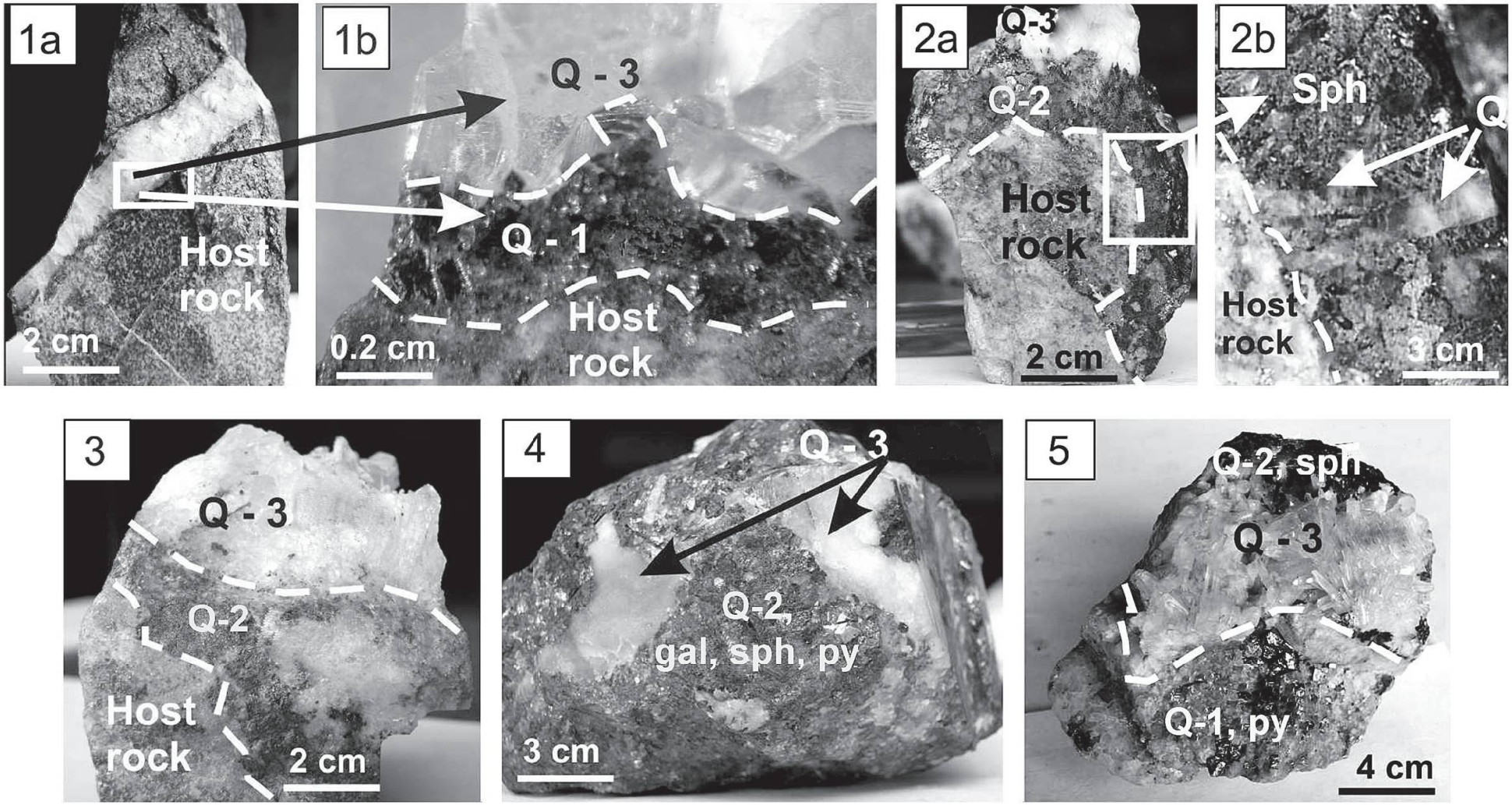

Fig. 3 Typical relations between and forms of quartz from stages Q1–Q3.
1a, 1b. Level 970 (vein), sample 62. Host rock (altered gneiss); quartz Q1 with chlorite and epidote as syngenetic inclusions; later quartz Q3;
2a, 2b. Level 1070 (vein), sample 173. Host rock (altered gneiss); quartz Q2 and ore minerals, mainly sphalerite; later quartz Q3;
3. Level 1020 (vein), sample 205. Host rock (altered gneiss); quartz Q2 and ore minerals – sphalerite, galena, pyrite; later Q3 quartz crystals (up to 2.5 cm) with small sphalerite as syngenetic inclusion;
4. Level 820 (vein), sample 28. quartz Q2 with mainly galena and some sphalerite, pyrite; overgrown by later clear Q3 quartz crystals.
5. Level 770 (skarn), sample 114. Q1 with pyrite; Q2 mainly with sphalerite; Q3 quartz crystals up to 1 cm.

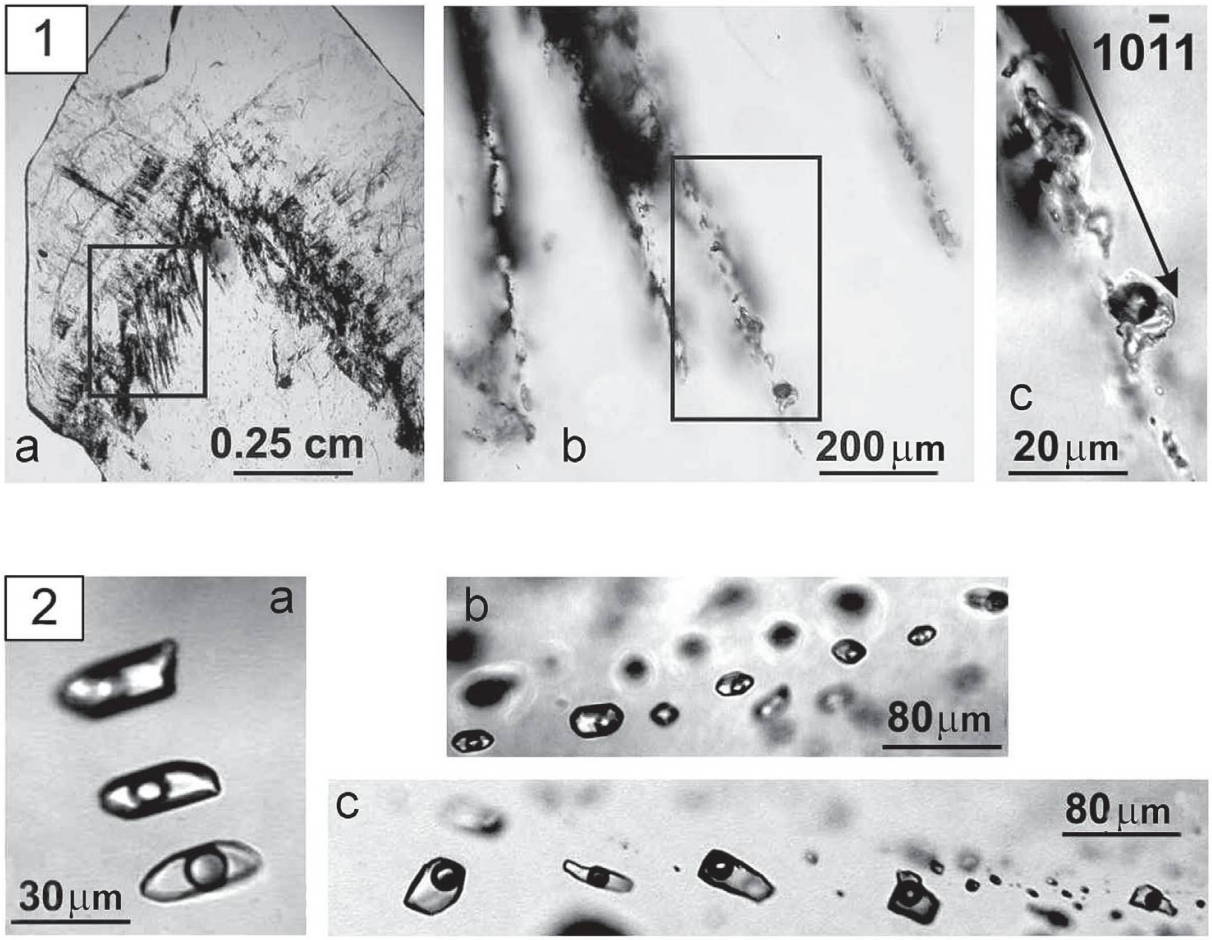

Fig. 4 (1) Primary sectorial fluid inclusions (level 931, N 282). (2) Pseudosecondary fluid inclusions; 2a: Level 970, N 62; 2b: Level 820, N 28; 2c: Level 668, N 269.

Our petrographically well-characterized samples (Fig. 3) represent the stages (1), (3), and quartz that crystallized after the sulphide ore minerals but probably before stage (5), as late generation of quartz from stage (3). We will use the notation Q1, Q2, and Q3 to distinguish these three paragenetic types. In order to relate fluids to the characteristic mineralization stages, we selected mainly fluid inclusions that petrographically can be characterized as "pseudosecondary", which are typically 20–60 micrometer in size and much larger than the locally present but generally small primary inclusions (Fig. 4). Only in one case, primary "sectorial" fluid inclusions (Petrov, 1981) could be analyzed. Selection of these types of inclusions ensures that the respective fluids were trapped during a particular stage of crystal growth. A total of 107 fluid inclusions from 11 doubly polished quartz sections were studied.

Our prototype LA ICP-MS system uses a 193-nm ArF excimer laser with output energy of 200–230 mJ. A stream of He gas transports the ablated material from the sample chamber and is mixed with Ar before entering the ICP quadrupole mass spectrometer (Elan 6100, Perkin-Elmer). Element concentration ratios were calculated by referencing intensity integrals against signal from external standards (NIST 600 silicate glass). These ratios were then converted to absolute concentrations using Na as an internal standard. The concentration of Na in fluid inclusions was calculated from their apparent salinity (measured by microthermometry) and the relative abundance of other major cations (from LA ICP-MS), using an empirical correction (Heinrich et al., 2003). A total of 26 major and trace elements in the hydrothermal fluids were analyzed.

Results

Temperature distribution with depth and mineralization stage

A plot of all homogenization temperatures against mining level shows an irregular distribution at first sight. However, if the temperatures are grouped by quartz stages Q1–Q3 (Fig.5), then those from the early Q1 show a distinctive, nearly linear trend with a gradient of about 40–50 °C/100 m.

Table 1 Laser ablation ICP-MS background-corrected analytical results. Analyses with the "<" sign has signals below limit of detection (LOD) as given by the respective number.

Stage	mine level, sample number	T_h [°C]	wt% $NaCl_{equiv}$	analysis number	Na^{23}	K^{39}	Cs^{133}	Rb^{85}	Sr^{88}	Mn^{55}	Sb^{121}	Zn^{66}	As^{75}	Pb^{208}	Tl^{205}
Q1 (quartz-pyrite)	**1128, 164**		4.94	ff13b06 (iii)	17256	5807	27	53	64	<343	<81	<286	<243	<54	<8.4
			4.78	ff13b07 (iii)	17229	4200	57	61	90	<159	83	<186	<132	<32	<9.7
			5.25	ff13b09 (iii)	19920	1955	67	44	38	129	<18	<63	<65	<13	<1.7
			4.78	ff20b05 (ii)	17269	3901	87	34	93	<315	<59	<312	<189	<43	<15.2
			4.45	ff20b06 (ii)	16719	2638	26	28	18	<144	<22	<65	<86	<18	<4.3
			4.45	ff20b07 (ii)	16241	1439	21	14	6	<123	43	<137	<108	<16	<6.3
			4.78	ff20b08 (ii)	16893	1663	62	35	18	<125	<23	<124	<76	<14	6.2
	1031, 3	274	4	ff13a03 (iii)	13762	4029	55	70	40	234	<10	90	<25	18	2.7
		274	4.2	ff13a05 (iii)	13547	6781	32	55	77	219	47	113	<80	44	<3.0
		279	3.1	ff13a07 (ii)	10746	3180	52	50	17	175	<11	<37	50	8	<1.4
		280	4.2	ff13a09 (ii)	13619	2599	65	38	30	197	<67	<183	158	<43	<6.2
		275	6	ff13a12 (ii)	20206	7306	67	59	35	120	<40	631	<93	29	<5.2
		275	5.8	ff13a13 (ii)	19491	6891	104	115	60	1832	34	138	22	30	5.4
		280	5.8	ff13a15 (ii)	18406	4878	12	<65	37	<637	<238	<1104	<468	<158	<25.0
		280	4	ff13b03 (ii)	14060	4469	32	53	12	207	60	<127	<100	<25	8.2
	970, 62	284.3	4.45	ff20a04 (iii)	15148	811	19	29	<1	<52	18	342	<32	21	<2.7
		296.1	5.85	ff20a05 (iii)	21684	1458	19	9	<1	<27	202	41	116	<6	<1.4
		297.3	4.63	ff20a06 (iii)	15962	191	27	5	5	33	224	<28	81	<5	<1.8
		296.4	4.45	ff20a07 (iii)	15302	72	18	7	<1	57	470	<29	141	<4	<1.3
		282.5	5.8	ff20a08 (iii)	17895	<54	4	<1	<1	<29	505	<29	129	<4	<0.6
		299	4.6	ff20a09 (iii)	16014	<24	13	4	0	<15	164	<16	103	<2	<0.7
		298	4.6	ff20a11 (iii)	13517	1751	41	24	3	171	231	<58	109	<6	<3.0
		292	4.6	ff20a12 (iii)	17766	281	36	8	9	<14	76	<13	34	<2	<0.4
		292	4.45	ff20a13 (iii)	15339	64	25	4	0	<12	201	<12	108	<2	<0.5
		292	5.8	ff20a14 (iii)	17679	<119	31	14	<2	<64	388	<58	206	<8	<2.0
	931, 282	263	5.55	ff20c03(primary FI)	20366	3913	81	76	65	298	<9	<35	<28	30	2.9
		253	5.85	ff20c05(primary FI)	21058	5215	74	82	28	91	<12	<33	<28	<7	3.4
		281	5.85	ff20c06(primary FI)	21052	5231	89	108	28	123	<13	<41	<33	<7	<3.4
		330	3.05	ff20c08 (ii)	9236	2995	32	34	14	28	19	<12	13	<2	1.2
		324	3.05	ff20c09	10907	2910	38	47	16	128	<1	11	<4	4	3.0
		328	3.05	ff20c10	11240	2024	8	21	<3	<54	<11	<35	<27	<7	<1.6
	865, 69a	320	3.53	ff13c03 (ii)	13217	1786	18	11	13	<9	<3	<11	<9	14	0.5
		320	4	ff13c04 (ii)	15030	1881	73	14	36	33	<6	<28	<18	10	0.5
		318	3.69	ff13c06 (ii)	13955	1496	33	16	18	<25	<8	<31	24	<5	<1.2
		319	4	ff13c07 (ii)	14807	2478	45	16	26	<38	<11	<45	<46	<9	<2.2
		320	4	ff13c10 (ii)	14606	3014	50	41	50	135	<57	<23	<16	<4	0.9
		320	4	ff13c15 (ii)	15421	841	13	11	22	<29	38	80	<23	<6	<1.4
		318	4	ff13c09 (iii)	10685	1896	16	12	51	36	67	<11	35	<2	<0.6
		320	3.53	ff13c13 (iii)	12657	2143	14	28	32	20	15	<8	16	<1	0.6
		320	4	ff13c14 (iii)	13552	1360	34	14	29	46	<10	<45	<29	<7	<2.0

Table 1 continued.

Stage	mine level, sample number	T_h [°C]	wt% $NaCl_{equiv}$	analysis number	Na ^{23}	K ^{39}	Cs ^{133}	Rb ^{85}	Sr ^{88}	Mn ^{55}	Sb ^{121}	Zn ^{66}	As ^{75}	Pb ^{208}	Tl ^{205}
Q2 (qtz-gal-sph)	**1070, 173**	293	3.9	ff05a03	12457	992	58	18	23	216	23	<9	22	3	1.4
		289	3.7	ff05a06	9131	2110	33	28	18	40	51	<9	<14	<4	1.3
		289	3.7	ff05a08	9709	2851	40	34	8	219	31	<19	<60	<14	<4.2
		290	3.9	ff05a04	12794	509	64	19	27	191	33	7	18	<2	0.9
		290	4	ff05a10 (+Ser)	12694	2675	47	43	12	72	279	6	30	1	1.4
	668, 269	318	4.79	ff13d03	18040	2144	110	58	33	413	<3	35	<10	17	3.5
		310	3.69	ff13d05	13215	3471	76	76	26	305	<5	<22	<17	7	2.0
		314	4.79	ff13d07	18543	801	75	27	24	280	<2	32	<6	8	1.8
		318	4	ff13d08	14832	2411	26	32	0	32	<3	<15	<8	7	<0.8
Q3 (late quartz)	**1020, 205**	295	6.72	ff11a03	24065	4672	113	92	69	665	<2	42	40	13	3.9
		290	6.68	ff11a06	22579	3375	88	69	27	101	9	<7	40	12	3.1
		290	6.68	ff11a07	23951	4592	87	78	60	476	22	5	16	3	4.0
		290	6.72	ff11a08	23644	4417	114	61	37	395	<3	<9	<9	10	5.4
		295	6.72	ff11a09	23845	5117	134	104	73	741	<1	17	35	10	4.7
		290	6.72	ff11a10	23947	5008	102	94	54	606	<2	15	32	10	3.7
		290	6.68	ff11a11	22298	7441	114	123	83	787	<4	<13	<11	4	5.8
		290	6.68	ff11a12	22606	5490	109	99	92	740	<10	<41	<35	<8	4.7
		291	6.72	ff11a13 (+Ser)	23705	5609	92	84	87	444	<2	<9	<7	5	3.8
		291	6.72	ff11a14	23889	3737	119	82	76	582	<3	<9	24	2	4.1
		305	6.68	ff11a15 (ii)	16336	9808	139	126	33	249	<9	<35	<26	<7	2.5
		304	6.72	ff11a16 (ii)	20553	6549	112	103	39	395	<2.8	<14	<9	<3	5.5
	931, 57	289	7	ff11b07(cracked)	27208	881	91	33	46	983	225.3	410	79	43	10.9
		291	6.9	ff11b08(cracked)	26790	945	102	40	13	862	192.9	433	51	48	4.5
		291.8	6.9	ff11b04	26319	2202	113	65	59	528	27.0	126	45	29	1.5
		289	7.6	ff11b09	29508	1041	101	43	13	595	256.8	522	105	21	1.7
		291	7.3	ff11b10	28419	797	115	67	9	706	110.9	156	94	36	4.3
		291	7.3	ff11b11 (ii)	28093	1668	95	47	34	649	<6.8	72	<18	23	3.7
	820, 28	289.6	5	ff11c04	19529	376	72	12	4	299	71.8	<32	38	<5	<1.5
		287.9	4.95	ff11c05	19384	238	65	18	<1	227	62.2	<22	25	<4	<1.6
		297.3	4.95	ff11c07	18859	1638	45	11	130	<36	<10.0	<35	<29	<7	<1.8
		291.3	4.6	ff11c03	16484	4300	63	69	16	103	<25.2	<87	<62	<13	<6.6
	770, 114.1	295	8.53	ff11d03(cracked)	29424	9204	176	110	98	473	157.5	252	<182	<36	<11.4
		280	7.99	ff11d05	29087	3134	178	162	65	406	<103.8	<283	<269	<60	<18.7
		282	7.99	ff11d06	25505	10704	163	161	54	448	35.9	25	23	<4	4.4
		284	7.85	ff11d07	28028	5400	107	92	91	125	18.2	14	<6	3	4.7
		284	7.99	ff11d09	28950	5678	101	123	88	1210	57.7	54	<29	13	<2.7
		284	7.85	ff11d10	24959	11024	78	72	71	824	50.3	191	<35	46	3.6
		290	8.53	ff11d12	29832	807	105	35	26	580	65.0	33	41	11	2.5
		282	7.85	ff11d08 (ii)	26459	9270	119	117	59	327	23.6	207	<55	63	4.8

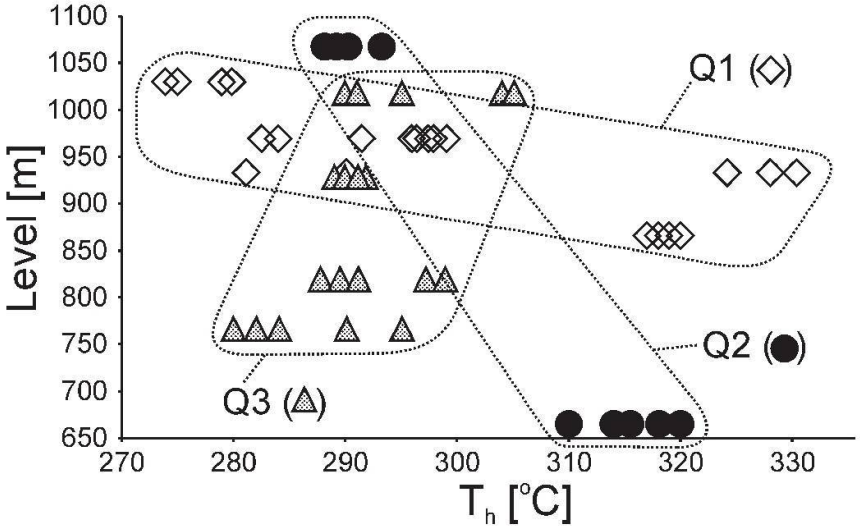

Fig. 5 Fluid inclusion homogenization temperatures vs. mine level for the three quartz stages.

For Q2, only two data sets are available with a vertical difference of 400 m, which indicate an upward temperature drop by 25 °C. If these are representative for the trend in Q2, the thermal gradient would have been much less pronounced than during the Q1 stage. In other words, the shallower parts would have been much hotter at this later stage than during Q1.

The Q3 data from the lower levels are shifted to lower temperatures compared with Q2, and only the data from the rather high level 1020 overlaps with those of Q2. The temperature during this stage seems rather independent of mining level, or even indicates a slightly cooler lower part implying an inverse thermal gradient.

Fluid composition

Most of the analyzed trace elements were below the limit of detection (LOD; Sn typically <5–30 ppm, Sc <1–30 ppm, Ag <1–10 ppm, Ge <10–30 ppm, Bi <1–2 ppm, Cd <20–60 ppm, Cu <5–100 ppm, Fe <100–1000 ppm, B <200–1500 ppm). Only Na, K, Rb, Cs and Sr are above detection limit throughout. Ca, Ba, Mn, Sb, As, Tl, Pb and Zn do at least in some samples show significant and quantifiable signals, which are summarized in Table 1.

The interpretation of strong Li and Al raw signals is difficult due to a strong variation of their contents in the host quartz, which dominates their yield in the ablation signal. Al is probably close to equilibrium between the fluid and feldspars + micas in the host rock (see below) and can be assumed to be rather low and below the typical detection limit. Nevertheless, host-corrected analytical results on fluid inclusions sometimes showed still very high Al contents up to several percent. We consider this an artefact resulting from the usage of low-Al zones in the host quartz for host correction, and have therefore assumed that Al in the fluid is generally below detection in all inclusions. In addition, it was found that the ratio of Al/Li in the host quartz and fluid inclusion raw analysis is very similar (17:1 to 20:1 on a ppm basis), which implies that the Li results are also dominated by the host quartz contribution. In these cases, Li was manually host-corrected by taking the raw Li value and subtracting Al(raw)/(average Al/Li ratio). In all these cases, Li values fell below LOD.

Ca is below the rather high detection limit of several thousand ppm in Q1, and occasional signals in Q2 and Q3 are too close to LOD to be considered as reliable. Mn is seen in concentrations of hundreds of ppm in most samples.

Of the ore metals, Pb and Zn mostly are below LOD in Q1. In Q2, both elements are detectable in the sample from the lowest level 668, with Pb at an average 8 ppm (ranging from 7 to 17 ppm), and Zn with 33 ppm, close to its LOD. At the 1070 m level, both elements are close to or below the LOD, and the few significant signals for Pb indicate about 2 ppm and about 6–7 ppm for Zn. In Q3, contents are generally significant, with Pb at typically 5–12 ppm at the highest level (1020 m), and even 30–50 ppm at 931 m. At the 770 m level, LOD vary substantially (up to 60 ppm) but where significant, Pb contents are in the range of 10 to >40 ppm. Zn values from 1020 m are mostly at the LOD and occasional successful results indicate concentrations of 5 to 40 ppm. Concentrations are very high at the 931 m level with 100 to 400 ppm and range from 14 to >200 ppm at the 770 m level. Copper signals are usually below LOD and the significance of occasional values in the range of tens of ppm is unknown. Significant signal of As, Sb and Tl appear

mainly in Q3, in agreement with the late appearance of arsenopyrite and sulphosalt minerals in the Madan ore deposits.

Discussion

Hydrodynamic model: temperature–space evolution

While the temperature vs. depth trends may seem unusual at a first glance, they are likely to represent a real evolution in the Yuzhna Petrovitsa hydrothermal system. Very similar trends were reported by Hayba and Ingebritsen (1997, see their figure 4) in simulations of hydrothermal fluid flow around cooling plutons. These authors simulated hydrothermal convection around a pluton as a function of host rock permeability. The hottest hydrothermal systems developed with host rock permeabilities around 10^{-15} m^2. Above the pluton, the hydrothermal system first establishes a steep thermal gradient (or a rather small slope if temperature is plotted on the horizontal and depth on the vertical axis) until after about 6000 years the system has developed a temperature-depth profile that corresponds to hot hydrostatic head conditions. This remains largely unchanged until, about 10'000 years after intrusion emplacement, the lower part of the system begins to cool faster than the upper part because the laterally recharging cold fluid cannot anymore be heated sufficiently by the cooled pluton. As a result, a negative temperature slope develops while there is a general cooling trend in the overall system.

The trends in the Yuzhna Petrovitsa fluid inclusion homogenization temperatures quantitatively match the general trends predicted by Hayba and Ingebritsen (1997) at a depth interval of around 1200–700 m (Fig. 6). This depth range is in excellent agreement with earlier estimates based on geomorphological, geological, and fluid state considerations as outlined by Bonev (1977) and Piperov et al. (1977). The Q1 data match the "heating up" phase about 4000–5000 years after intrusion, Q2 records the period between about 5000 and 8000–9000 years under hot hydrostatic head conditions in a boiling fluid column, and Q3 represents the situation about 10'000 years after intrusion. It is not clear if the apparent negative thermal gradient in the fluid inclusion data really does reflect the actual state of the system at one specific time. It may rather result from trapping of fluids at slightly different times at different depths since a negative thermal gradient would not allow quartz precipitation and trapping of fluid inclusions. It is nevertheless in very good agreement with the overall evolution of an apparently normal magmatically heated hydrothermal system.

This scenario is also in agreement with Bonev et al. (1993), who interpreted their stable isotope data in terms of a hydrothermal convection system above a cooling magma body. Hayba and Ingebritsen's (1997) simulations indicate that hydrothermal systems with these temperature-depth relations develop only for a very restricted range of bulk (>100 m scale) permeabilities around 10^{-15} m^2. They did, however, not investigate the role of fractures in the system and how this changes the temperature evolution, nor the effects of focussing of fluids in the third dimension (i.e. within the fault plane). It should also be noted that the timing given in their paper is for a rather small intrusion of 1 km width with a top at 2 km depth, but this does not imply that these numbers pertain directly to the Madan case. A larger pluton would require a longer cooling period. In spite of the quantitative agreement with the Hayba and Ingebritsen (1997) results, we cannot yet decide whether this does imply that the system formed above a cooling pluton. Radiogenic isotope dating of various stages of the evolution of the Madan Dome has shown a very rapid change in temperature from migmatic conditions to lower greenschist facies in about 5 Ma or less for present day surface outcrop in the lower plate of the Dome (see Kaiser-Rohrmeier et al., 2004, and references therein). This implies a strong thermal gradient in the host rocks, which could potentially lead to a similar overall circulation and cooling pattern even in the absence of a magmatic intrusion. On the other hand, widespread rhyolitic dikes with ages similar to those of the hydrothermal activity may be indicators for larger magmatic bodies at depth.

Ore metal solubilities: analysis and thermodynamic prediction

The general chemical characteristics of most of the analyzed quartz-hosted fluid inclusions are in very good agreement with those observed by Piperov et al. (1977) by direct extraction and analysis of primary fluid inclusions in galena. There are however, some differences that reflect the broader range of mineralization stages covered by our analysis.

Average Na contents of 1.2 to 1.8 wt% and K of >0.2 wt% in Q2 overlap nicely with the galena-hosted inclusions. Na contents do significantly increase to >2% in Q3, in agreement with the generally higher salinity of the Q3 fluids indicated by microthermometry. A similar picture is seen for K, as well as for Rb and Cs for which no data from

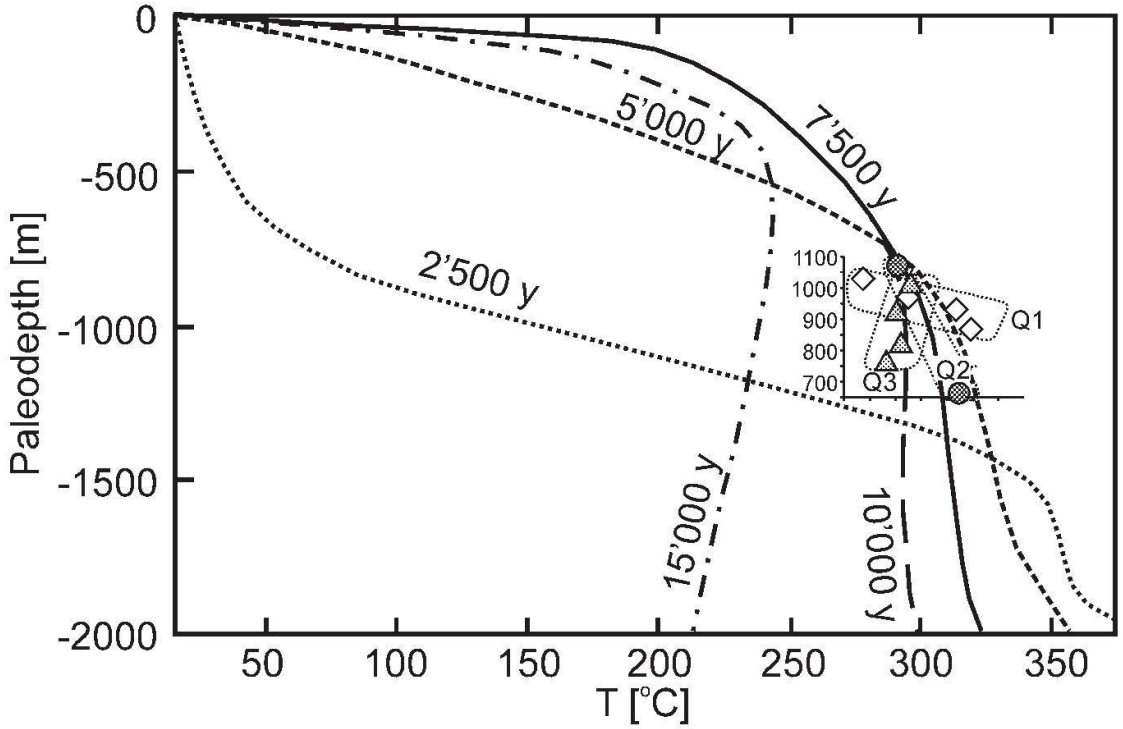

Fig. 6 Data from Figure 5 plotted on data from hydrodynamic simulations of fluid flow above a cooling pluton (modified from Hayba and Ingebritsen, 1997). For the sake of simplicity, only the average homogenization temperature of each data set from Figure 5 was plotted.

galena-hosted inclusions are available. Manganese values generally match the range of the Piperov et al. (1977) data, while their Ca, Fe, and Mg data indicate contents below our LOD.

In general, we conclude that the fluid inclusions that were assigned to Q2 for petrographical reasons, are chemically very similar to those known to be primary inclusions in the ore minerals. Therefore, the measured ore metal contents are likely to reflect those present during ore formation.

The solubility of galena and sphalerite from hydrothermal solutions is controlled by reactions of the kind

$$PbS + nCl^- + 2H^+ = PbCl_n^{2-n} + H_2S \quad (1)$$
$$ZnS + nCl^- + 2H^+ = ZnCl_n^{2-n} + H_2S \quad (2)$$

i.e., the main solubility-controlling parameters are chloride activity, pH and total reduced sulphur, m_{Stot}. High salinity, low pH and low molality of total reduced sulphur ($H_2S_{(aq)} + HS^-_{(aq)} + S^{2-}_{(aq)}$), m_{Stot}, favour the solubility, of which salinity has the largest influence since solubility runs with power n (n from the above reactions is typically 3 for Pb and 4 for Zn under the conditions of interest; Seward, 1984; Ruaya and Seward, 1986). The total Pb or Zn in the fluid is known from the LA-ICPMS analyses, and chloride activity can be obtained from the fluid inclusion results as well. pH and total reduced sulphur are unknown but can be constrained from ore mineral and alteration assemblages (see below).

The measured lead and zinc concentrations can thus be compared with theoretical and experimental studies. Barrett and Anderson (1988) gave approximate formulae for calculating the solubilities of galena and sphalerite in brines. We take 1 m brine as an approximation for the Madan ore fluid and 7–8 ppm Pb and 33 ppm Zn as an average for fluids at the bottom of the system during Q2 (sample 269 from the 668 m level). From the 668 m level to the 1070 m level, we see a drop in homogenization temperature by about 25 °C. Interpolating the formulae of Barrett and Anderson (1988), at galena or sphalerite saturation, respectively, this would lower the concentration of Pb in the fluid by about 85%, and that of Zn by about 80%, predicting 1.2 ppm of Pb and 6.6 ppm Zn at 1070 m. This is in very good agreement for the two significant measurements of 1 and 2 ppm for Pb and 5 ppm for Zn with all other analyses having a LOD higher than these theoretical concentrations. Overall, this indicates that the observed lower concentration at 1070 m is likely to be the result of galena and sphalerite precipitation by cooling over this 400 m interval.

The cooling occurs along a "boiling curve with depth" path. Based on this observation Bonev (1977) and Piperov et al. (1977) concluded that fluid boiling and subsequent pH increase due to the loss of CO_2 to the vapour phase was likely the most important precipitation mechanism. A decision about the relative importance of cooling along the boiling curve vs. pH changes due to the

boiling scenarios will only be possible on the basis of a detailed and accurate thermodynamic analysis, which is beyond the scope of this study.

The chemical conditions during ore precipitation can be constrained quite narrowly. An estimate of pH is possible from the alteration assemblages in the deposit. In the gneissic host rocks, K-feldspar is typically altered to sericite (muscovite), which frequently also occurs as a late gangue mineral on the sulphides. The stability boundary between muscovite and K-feldspar occurs at $\log(a_{K+}/a_{H+})$ around 4 at 300 °C (using the Supcrt92 data, Johnson et al., 1992). The lower pH limit is constrained by the stability of muscovite against kaolinite at $\log(a_{K+}/a_{H+})$ of around 2. The total K concentration is known as being around 0.25 to 0.3 % (i.e., < 0.1 molal). For these low concentrations, association to ion pairs KCl^0 in the solution is negligible and K^+ concentration is identical to the analytical one. Using an extended Debye-Hückel type activity law, the activity of K^+ in the solution would be in the order of 10^{-2} and, hence, pH must have been in the range of approximately 4 to 6. Rearranging Barrett and Anderson's (1988) formulae and using the concentrations given above gives a pH–m_{Stot} relation for galena and sphalerite saturation that follows the equation $\log(m_{Stot}) = 7.4–2$ pH. This relation helps us to further constrain the pH range: if we assume that m_{Stot} >0.1 are unlikely, galena and sphalerite would be undersaturated at all pH <4.2. A lower limit of m_{Stot} is given by the lower stability of pyrite vs. pyrrhotite. Using standard thermodynamic data from the Supcrt92 database (Johnson et al., 1992), we calculate a $\log(m_{Stot})$ of about –2.95 at the pyrite–pyrrhotite equilibrium, assuming H_2S and HS^- as the major aqueous reduced sulphur species at a typical hydrogen fugacity of 0.1 bar and that oxidized sulphur species are negligible. Therefore, and if the Barrett and Anderson solubilities are reliable, the maximum pH at which the observed solubilities were possible at 310 °C would be around 5.2, which is in very good agreement with the 4.6 to 6.2 of Piperov et al. (1977) derived from primary inclusions in galena. Our calculated value is subject to several uncertainties, probably mainly in the correlations of Barrett and Anderson (1988), and needs further refinement by more rigorous thermodynamic calculations including the most reliable speciation models available. Nevertheless, a slightly acidic fluid with pH below that of the K-feldspar–muscovite–quartz is in agreement with the field observation that all feldspar in rock fragments within the veins or in the wall rock immediately adjacent to the vein is altered to white mica.

Inclusions in Q3 quartz post-date the main ore stage and show higher salinity, which will increase the solubility of the ore metals dramatically. In a first-order stoichiometric approximation, the salinity increase by a factor of about 1.8 would lead to an isothermal solubility increase for galena by $1.8^3 = 5.8$, and for sphalerite by $1.8^4 = 10.5$ (see above), which is in fair agreement with the LA-ICPMS data, taking a reduction of solubility due to the somewhat lower temperature compared to Q2 into account. Increased solubility due to slight salinity increase in the late fluids is in excellent agreement with the dissolution textures frequently seen on galena crystals at Madan. If the relative durations of the various stages in the thermal evolution of the system followed the trends in the simulations of Hayba and Ingebritsen (1997), this stage would be rather short and highly transient in comparison to the preceding ore-forming stage, thus explaining why any ore minerals are left at all.

Estimate of fluid amount

The economic content of lead in the Madan ore field produced so far is >2 Mt. Assuming this amount of metal together with an average Pb concentration in the incoming ore-forming fluids of 10 ppm (slightly higher than sample 269 from the 668 m level), and assuming 100% precipitation efficiency as a conservative constraint, the minimum amount of ore fluid that must have flown through the system during the quartz–sphalerite–galena mineralization stage would have been 2×10^{11} t of water, or about 200 km^3. This is of the same order of magnitude as the 130 km^3 of dominantly meteoric fluid estimated for the active Wairakei geothermal system in New Zealand, based on a discharge rate of ~400 kg/s (Fisher, 1964) and assuming a lifetime of 10'000 y for its current hydrothermal event. Wairakei covers a significantly smaller area than the Madan ore field, which makes the estimated number seem even more plausible. A purely meteoric origin of the fluid seems to contrast the amount of chloride that passed through the system. Whether or not the chloride is derived from magmatic or other sources remains speculative. Also, the D/H and $^{18}O/^{16}O$ data of Bonev et al. (1993) are rather inconclusive in this respect because the observed trends may equally well be interpreted as fluid-rock interaction paths of purely meteoric fluid or mixing lines between meteoric and magmatic fluids.

Conclusions

The combination of microthermometric and LA-ICP-MS results from fluid inclusions with published thermodynamic and hydrodynamic models

has provided new quantitative insight into the thermal and chemical evolution of the hydrothermal system that formed the Yuzhna Petrovitsa Pb–Zn deposit. The thermal evolution reconstructed from the microthermometric data does quantitatively match predictions from hydrodynamic fluid flow simulations and hence shows that pseudosecondary fluid inclusions – if selected on the basis of careful petrography – are an important means for quantitative fluid inclusion studies. The reliability of our results is further supported by the agreement between LA-ICP-MS results on quartz-hosted inclusions that petrographically belong to the main ore stage and published chemical analysis of macroscopic primary fluid inclusions in galena.

The LA-ICP-MS results let us conclude that the main mechanism of ore deposition in the vein was a gradual cooling of upwelling fluids by about 25 °C over a ~400 m vertical interval, leading to precipitation of 80–85% of the initial Pb and Zn content of the fluid. We did not investigate the zoning of metal ratios or the mechanism of ore precipitation in the replacement ore bodies, which is probably dominated by fluid-rock interaction with marble and/or manganese skarn minerals. If we assums that the fluid evolution at Yuzhna Petrovitsa is representative for the whole Madan district, mass balance calculations based on the analyzed ore metal contents in the fluid inclusions indicate a fluid volume in the order of 10^2 km^3 for the formation of the whole Madan district, which is well within the range of time-integrated fluid amounts known to pass through currently active hydrothermal systems within a lifetimes of 10^4 years.

Acknowledgements

The constructive reviews by I. Bonev and P. Barton helped to improve the quality of this paper. This study was supported by SCOPES grant nr. 7BUPJ062396 of the Swiss National Science Foundation.

References

Barret, T.J. and Anderson, G.M. (1988): The solubility of sphalerite and galena in 1–5 m NaCl solutions to 300 °C. *Geochim. Cosmochim. Acta* **52**, 813–820.

Bonev, I.K. (1977): Primary fluid inclusions in galena crystals. I. Morphology and origin. *Mineralium Deposita* **12**, 64–76.

Bonev, I.K., Boyce, A.J., Fallick, A.E. and Rice, C.M. (1993): Stable isotope evidence for the genesis of the Madan vein and replacement lead–zinc deposits, Central Rhodopes, Bulgaria. In: Fenoll Hach-Ali, (ed.): Current research in geology, applied to ore deposits, Granada, 37–40.

Bonev, I.K. and Kouzmanov, K. (2002): Fluid inclusions in sphalerite as negative crystals: a case study. *Eur. J. Mineral.* **14**, 607–620.

Fisher, R.G. (1964): Geothermal heat flow at Wairakei during 1958. *New Zealand J. Geol. Geophys.* **7**, 172–184.

Günther, D., Audetat, A., Frischknecht, R. and Heinrich, C.A. (1998): Quantitative analysis of major, minor and trace elements in fluid inclusions using laser ablation inductively coupled plasma mass spectrometry. *J. Analytical Atomic Spectrometry* **13/4**, 263–270.

Hayba, D.O. and Ingebritsen, S.E. (1997): Multiphase groundwter flow near cooling plutons. *J. Geophys. Res.* **102**, B6, 12235–12252.

Heinrich, C.A., Pettke, T., Halter, W.E., Aigner-Torres, M., Audetat, A., Günther, D., Hattendorf, B., Bleiner, D., Guillong, M. and Horn, I. (2003): Quantitative multi-element analysis of minerals, fluid and melt inclusions by laser-ablation inductively-coupled-plasma mass-spectrometry. *Geochim. Cosmochim. Acta* **67**, 3473–3497.

Ivanov, Z., Dimov, D. and Sarov, S. (2000): Structure of the Central Rhodopes. ABCD–GEODE 2000 workshop, Borovets, Bulgaria, Guide to excursion (B), 6-20.

Johnson, J.W., Oelkers, E.H. and Helgeson, H.C. (1992): SUPCRT92: A software package for calculating the standard molal thermodynamic properties of minerals, gases, aqueous species, and reactions from 1 to 5000 bar and 0°C to 1000°C. *Computers Geosci.* **18**, 899–947.

Kaiser-Rohrmeier, M., Handler, R., von Quadt, A. and Heinrich, C.A. (2004): Hydrothermal Pb–Zn ore formation in the Central Rhodopian Dome, south Bulgaria: Review and new time constraints from Ar–Ar geochronology. *Schweiz. Mineral. Petrogr. Mitt.* **84**, 37–58.

Kolkovski, B. and Dobrev, S. (2000): Ore mineralization in the Central Rhodopes. ABCD–GEODE 2000 workshop, Borovets, Bulgaria, Guide to excursion (B), 21–36.

Kolkovski, B. and Petrov, P. (1972): On the temperature of ore-forming in deposits along the Spolouka-Laikov Choukar fault, Madan district. *Ann. Univ. Sofia, Geol.* **64/1**, 225–233 (in Bulgarian).

Ovtcharova, M., von Quadt, A., Peytcheva, I., Cherneva, Z., Neubauer, F., Rohrmeier, M. and Heinrich, C.A. (2001): Acid magmatism in the Madan core complex (Central Rhodope, Bulgaria) – new isotope and geochronological data. Abstract, ABCD–GEODE 2001 workshop Vata Bai, Romania.

Petrov, P. (1981): Primary sectorial fluid inclusions in milky-white quartz. *C. R. Bulg. Acad. Sci.* **35/4**, 487–490.

Piperov, N.B., Penchev, N. and Bonev, I. (1977): Primary fluid inclusions in galena crystals. II. Chemical composition of the liquid and gas phase. *Mineralium Deposita* **12**, 77–89.

Piperov, N.B. and Penchev, N. (1982): Deuterium content of the inclusion water from hydrothermal galenas, Madan, Bulgaria – preliminary investigation. *Econ. Geol.* **77 (1)**, 195–197.

Rohrmeier, M., von Quadt, A., Handler, R., Ovtcharova, M., Ivanov, Z. and Heinrich, C. (2002): The geodynamic evolution of hydrothermal vein deposits in the Madan metamorphic core complex, Bulgaria. Goldschmidt Conference Abstracts, A645.

Ruaya, J.R. and Seward, T.M. (1986): The stability of chlorozinc(II) complexes in hydrothermal solution up to 350°C. *Geochim. Cosmochim. Acta* **50**, 651–661.

Seward, T.M. (1984): The formation of lead(II) chlorids complexes to 300°C: A spectrophotometric study. *Geochim. Cosmochim. Acta* **48**, 212–134.

Received 19 December 2003
Accepted in revised form 22 October 2004
Editorial handling: A. von Quadt